Tribo-rheometry: from gap-dependent rheology to tribology

H.P. Kavehpour and G.H. McKinley
Hatsopoulos Microfluids Laboratory
Department of Mechanical Engineering
Massachusetts Institute of Technology, Cambridge, MA, USA

August 19, 2003

Abstract

We describe a new triborheometry fixture that can be utilized with a commercial torsional rheometer in order to explore the coupled rheological and tribological properties of complex fluids and solid-liquid systems. The fixture is self-leveling and both the normal load and the sample gap can be monitored or controlled. At large gaps, the fixture imposes an approximately constant shear rate on the sample and the bulk viscometric properties of the fluid can be measured. However, as the gap between the plates is reduced, the measured viscosity function becomes gap-dependent. For gaps on the order of the surface roughness of the plates, the device is operated under a constant applied load and the tribological properties of the fluid-solid pair can then be measured. Using this new triborheometer fixture it is possible to obtain tribological information over a wider range of sliding velocities than is typically possible using conventional devices such as pin-and-disk systems. The data can be represented in the form of a classical Stribeck diagram or, by using a dimensionless gap-dependent shift factor, it is possible to construct a more general 'friction map' of the gap- and load-dependent effective viscosity (Luengo et al. Wear, **200**, 1996). The capabilities of this system are illustrated using a number of different lubricant fluids, for a range of normal stresses and variations in surface properties such as the mean roughness.

Keywords: Stribeck, friction, lubricity, gap-dependent rheology.
Running Head: Tribo-Rheology

1 Introduction

Tribology and rheology are typically regarded as distinct scientific disciplines. The rheological properties of a fluid govern the transmission of stresses between two distinct, and widely-separated, rigid bounding surfaces and characterize the associated viscous dissipation of energy in the flowing and deforming fluid medium. Tribological effects become increasingly important as the normal load on the system increases, and the separation of the solid surfaces decreases, towards the point of contact between asperities; with a progressive cross-over from hydrodynamic lubrication through mixed lubrication to boundary lubrication.

In many modern technological applications, however, the distinction between rheology and tribology is less clear. The system may involve micromachined structures, microfluidic flow channels or microstructured fluids and both the tribological and rheological properties can be important in controlling the frictional dynamics of the system. The complexity of these interactions in biological and microfabricated systems has been summarized in a number of recent monographs [1, 2, 3]. The composite response of the system involves interactions between the characteristic length scales of the device, the microstructure of the fluid and the characteristic roughness of the substrate [4, 5, 6]. Some specific examples in which both the rheological and tribological properties have been studied in detail include the analysis of polymeric lubricants for magnetic recording and aerospace applications [7], and the properties of consumer products and foods; recent tests have shown that user perception of 'texture' correlates in a complex way with both rheological and tribological tests [8, 9]. These complex tribological and rheological interactions are commonly captured through heuristic terms such

as 'lubricity' or 'lubriciousness'.

True rheological material functions are presented in terms of 'rheograms' (or plots of the fluid viscosity η as a function of the imposed shear rate $\dot{\gamma}$); whereas the tribological properties of a fluid-solid pair are typically represented as a Stribeck diagram of the coefficient of friction μ as a function of the sliding (or rotational) velocity V. Ideally, these apparently-distinct properties could be measured using a single device and represented as a single curve or family of curves. Such ideas were recently discussed in detail by Luengo et al. [10] who proposed a number of new 'friction maps' that conveyed both tribological and rheological information in the boundary lubrication regime and beyond. By using the sliding forces apparatus (SFA) with molecularly-smooth mica surfaces they obtained sliding friction data that could be interpreted as the effective viscosity η_{eff} of a molecularly-thin fluid film. This effective viscosity is orders of magnitude larger than the macroscopic or bulk viscosity, η, due to molecular-ordering and typically varies as $\eta_{eff} \sim \dot{\gamma}^{-n}$ with $1/2 \leq n \leq 1$. More recent summaries of the important role of 'nanorheology' and thin film lubrication in nanometer-scales gaps between molecularly-smooth plates are given by Granick and coworkers [11, 12]. It is not presently known how important such nanorheological effects are in flows involving other (typically larger) microstructural characteristic length scales; for example in fluids containing macromolecular components or in geometries with roughness scales characteristic of industrial finishing/polishing protocols.

Conventional cone-plate or parallel-plate rheometers and tribological devices such as pin-on-disk testers have a number of common design characteristics. In particular, they typically utilize torsional flows to constrain and contain the test fluid, they allow the attachment of

different test geometries and, finally, incorporate electromechanical subsystems with wide dynamic ranges in order to impose and/or measure known rotation rates, normal loads and torques on fluid samples. It is thus plausible to consider the design of a new test fixture that can generate both rheological and tribological data. In the present communication we introduce a simple design for a self-centering and self-leveling *tribo-rheometry* fixture which can be used in conjunction with a standard torsional rheometer. The sample dimension H can be smoothly varied from values characteristic of standard rheometry ($100\mu m \leq H \leq 2$ mm) down to values less than the characteristic roughness of the fixtures (i.e. to nominally a 'zero-gap' separation) under conditions of controlled normal load, $1N \leq F_N \leq 50N$. The resulting test data can be used to generate the familiar Stribeck diagrams and traditional rheograms as well as to extend the friction map ideas of Luengo et al. [10] to systems involving more rheologically-complex macromolecular or multiphase fluids and hard or soft bounding surfaces which are not atomistically smooth. In section 2 of this Letter we describe the design, fabrication and calibration of the tribo-rheometry fixture. In section 3 we show how the fixture can be used to construct Stribeck curves and more general friction maps over a wide range of parameter space, for a number of test surfaces of differing characteristic roughness and for a range of different test fluids. Preliminary experiments show that such tribo-rheometry fixtures may also be useful in future studies of biological lubrication and wear characteristics.

2 Design & Geometry

As noted in the introduction, the tribo-rheometer is a fixture that can be added to a commercial torsional rheometer to capture the tribological properties of the system (ie the frictional interactions of a fluid-surface pair) as well as the 'bulk' rheological properties of the fluid under shear. We used a torsional rheometer (AR-2000, TA Instruments Inc.) with a stainless steel parallel plate configuration as shown in figure 1. Due to the radial variation of the local shear stress τ in the parallel plate geometry, the cone and plate geometry is more suitable for traditional rheological measurements of complex fluids. The advantage of the parallel plate geometry is the ability to readily vary the gap size, H, as compared to the fixed cone angle of a specified conical fixture. Decreasing the gap H enables higher shear rates to be attained for the same fluid which is not possible with a cone and plate system. The lower bounding surface is a Peltier plate assembly which is used not only to control the temperature of the fluid sample, but also to measure the normal force acting on the surface using a force transducer that is mounted below the surface.

To obtain tribological properties using a torsional rheometer, a new *triborheometry* fixture is designed and installed on the surface of the Peltier plate. The simple design enables the user to interchange different hard or soft materials as the lower fixture in place of using the surface of the Peltier plate. This also eliminates the possibility of damaging the sensitive Peltier plate through wear. The parallelism of the upper and lower fixture surfaces can be adjusted using a self-aligning protocol described below.

We have developed two different test fixtures. The first generation tribo-rheological fixture

consists of a circular plate of chosen surface material with known physical properties such as surface roughness. To ensure the parallelism of the lower fixture with the upper rotating plate, a small amount of wax is deposited on the Peltier element. The temperature of the Peltier plate is increased to the melting point of the wax. The circular disk that forms the lower fixture is placed on the top of the wax layer. The top plate is brought down and a small normal force is applied to the fixture. The fixture surface is then forced to be in full contact with the top plate. By decreasing the temperature of the Peltier plate back to room temperature, the wax is solidified and the lower fixture remains rigidly attached to the substrate and in alignment with the top plate. The top plate can then be retracted using the rheometer drive system and is ready for loading of the liquid sample. A small amount of the test fluid (typically between 10-50 μl) is then deposited on the lower fixture and the top plate is moved down to the desired gap setting. When a torque, T, is applied to the top plate, the fixture reaches a certain constant angular velocity, Ω, which is measured by an optical encoder on the shaft. Through a feedback system available in the AR-2000 rheometer, one can design a test procedure that then varies the angular velocity over several orders of magnitude at either constant gap or constant normal force and measures the corresponding torque required for a specified velocity.

The shear rate, $\dot{\gamma}$, in the fluid sample resulting from the rotating top plate is simply $\dot{\gamma} = \Omega r/H$. The applied torque is found by integrating the shear stress, τ, acting on the rotating surface of the plate [13]. By changing variables in favor of the 'rim shear rate' at the edge of the fixture, $\dot{\gamma}_R = \Omega R/H$, and differentiating the expression for the torque the following relation for the viscosity of the fluid as a function of the rim shear rate is obtained

[13]

$$\eta(\dot{\gamma}_R) = \frac{T}{2\pi R^3 \dot{\gamma}_R}\left(3 + \frac{d\ln\left(T/2\pi R^3\right)}{d\ln\dot{\gamma}_R}\right), \tag{1}$$

where R is the radius of the top rotating plate and the shear stress is $\tau = \eta(\dot{\gamma})\dot{\gamma}$. This enables the rate dependence of the steady shear viscosity function to be determined directly from measurements of the torque and rim shear rate.

However, if the fluid is Newtonian, and the viscosity is not a function of deformation rate ($\eta \neq \eta(\dot{\gamma})$), then the torque is linearly related to the rim shear rate and this expression can be reduced to a simple relation between the applied torque, T, and the shear stress, τ_R, at the rim of the disk:

$$\tau_R = \frac{2}{\pi R^3}T = \frac{T}{SF_{PP}}. \tag{2}$$

The geometric term $SF_{PP} = 2/\pi R^3$ is usually called the "stress factor" which relates the applied torque to the shear stress. The viscosity of the fluid is then obtained directly from the shear stress or measured torque $\eta = \tau_R/\dot{\gamma}_R = 2HT/(\pi\Omega R^4)$.

If the gap is progressively decreased, the two surfaces eventually begin to contact each other resulting in a steady increase in the positive normal force or thrust exerted. Using a feedback loop in the rheometer, this applied normal force can be set and held at a constant value with an accuracy of ± 0.1 N. When the normal force is set, by running a similar velocity sweep procedure, one can measure the torques and subsequently the variation in the rim shear stress $\tau_R(\Omega)$ with angular velocity can be obtained. This enables us to generate a Stribeck diagram for the fluid-solid pair. In non-rotating systems, the dimensionless number of choice is the Sommerfeld number which is defined as $So = \eta V/P$, where V is the linear velocity

and P is the normal force per unit length of the contact. For rotating systems, the Gumbel number [1] is defined as:

$$Gu = \frac{\eta\Omega}{\sigma} = \frac{\eta\Omega\pi R^2}{F_N}. \tag{3}$$

where η is the shear viscosity, and $\sigma = F_N/\pi R^2$ is the average or nominal normal stress acting on the rotating plate. Knowing the preset normal force, the area of the plate, and fluid viscosity, the measured radial velocity can be converted to dimensionless values of the parameter Gu. The coefficient of friction, μ, is defined as the ratio of the shear stress, τ_R, to the normal stress, σ. By calculating the shear stress from the imposed torque using the stress factor for this geometry from equation(2), a Stribeck diagram can thus be generated.

This fixture is very simple to design, fabricate, and align, however an important approximation is made in the calculation of the shear stress. As noted above, the local sliding velocity and shear stress is not constant in a parallel plate geometry and varies linearly with radius, although the majority of the contribution to the total torque arises from fluid elements near the rim $r \approx R$. To minimize radial variations, we have also designed a second generation of tribo-rheometer fixture. The difference between this fixture and the design above is the use of an annular disk as the lower fixture as shown in figure 1.

The radial variation of the shear stress is reduced, however a new stress factor has to be used to convert the torque to the average shear stress exerted on the fluid by this configuration. The torque applied to the top plate is now given by:

$$T = 2\pi \int_{R_1}^{R_2} r^2 \tau\left(r\right) dr, \tag{4}$$

where $\tau(r) = \eta\dot{\gamma}(r)$ and the inner and outer radii of the disk are R_1 and R_2.

If $(R_2 - R_1)/R_1 \ll 1$ then the variation in shear rate across the annulus is small and the viscosity is constant at leading order. The torque is then given by:

$$T = 2\pi \int_{R_1}^{R_2} \frac{\eta \Omega r^3}{H} dr = \frac{2\pi \eta \dot{\gamma}_{\bar{R}}}{\bar{R}} \left(\frac{R_2^4 - R_1^4}{4} \right). \tag{5}$$

where an average shear rate $\dot{\gamma}_{\bar{R}} = \Omega \bar{R}/H$ can be defined based on the average radius of the annulus $\bar{R} = \frac{1}{2}(R_1 + R_2)$. Using this relation with equation (5) results in the following relationship between the average shear stress $\tau_{\bar{R}} = \eta \Omega \bar{R}/H$ and the measured torque

$$\tau_{\bar{R}} = \frac{2\bar{R}}{\pi(R_2^4 - R_1^4)} T. \tag{6}$$

The stress factor for this annular disk geometry is therefore $SF_{ann} = 2\bar{R}/\pi(R_2^4 - R_1^4)$. By using this new expression for the shear stress, a Stribeck diagram can again be constructed in the same manner as explained above.

Finally we note that both of these fixtures must be concentrically aligned with the axis of the upper rotating shaft in order to eliminate any eccentric effect. To facilitate this, we designed a simple centering frame with two concentric holes machined on each side. The larger hole has the same diameter as the Peltier plate, whilst the other groove has the same diameter as the fixture and is located exactly at the center of the Peltier plate. By placing the centering frame on the Peltier assembly and then locating the chosen fixture in the small groove, we ensure the effect of eccentricity is reduced to approximately 0.001" ($25\mu m$).

3 Results & Discussions

3.1 Gap-dependent rheology and cross-over to tribology

In this initial series of results, a first generation (circular) fixture of polished copper with radius $R = 10$ mm and mean surface roughness of $\epsilon = 678$ nm (measured using a surface profilometer; P10 Tencor Inc.), is used with a standard lubricant oil (Pennzoil 80W-90). The stress factor for this system is $SF_{pp} = 2/\pi R^3 = 0.64\text{cm}^{-3}$. The rotating top plate is a stainless steel plate with diameter of 2 cm. The gap, H, between the top plate and the fixture is set at 300μm. For a specified range of steady angular velocity, Ω, the required driving torques, T, are measured. This procedure is repeated for several other plate separations of 200μm, 100μm, 80μm, 50μm, and 20μm. The results, spanning five orders of magnitude of rotation rate, are shown in figure 2(a). As expected, these results do not superpose on each other due to the different gap settings. One can compute the viscosity of the fluid from these results using equation (1). The constant slope on this logarithmic plot indicates that over the range of shear rates tested the fluid can be treated as essentially Newtonian with little shear-thinning in the viscosity.

The gap is reduced further until the plates contact each other, and the normal force is now employed as the control variable. The normal force is specified and controlled at values of 5N and 15N, and angular velocity sweeps are again performed for these cases. These results are also presented in figure 2(a). At higher angular velocities, the measured torque on the top plate again varies linearly with rotation rate in similar fashion to the results obtained at finite

gap size with no preset normal force. However at a certain velocity, the torque deviates from this linear response and begins to increase when the angular velocity decreases. As shown in figure 2(a), this deviation does not occur for gaps larger than approximately 20μm. The linearly-increasing regions of these curves are characteristic of hydrodynamic lubrication and the regime in which the torque remains approximately independent of rotation rate is commonly known as the boundary lubrication regime. The two regions are connected via the mixed lubrication region.

Since we are using the same fluid for each of the experiment we can superimpose the hydrodynamic part of the tribology tests with the rheometric (finite gap) data by using a purely-geometric shift factor a_h to translate the curves horizontally along the abscissa. The simplest definition of this dimensionless shift factor is the aspect ratio, $a_h = R/H$, *i.e.* the ratio of the radius of the fixture to the specified gap setting. The product of rotation rate and the shift factor is then the rim shear rate, $\dot{\gamma}_R = \Omega a_h$. It was shown above that the viscosity of the fluid is related to the shear stress at this point as $\eta = \tau_R/\dot{\gamma}_R$, and furthermore τ_R is linearly related to the torque, T from equation (2). Therefore the slope of the curves in the hydrodynamic region is:

$$\frac{T}{\dot{\gamma}_R} = \frac{\pi R^3}{2}\eta = \frac{1}{SF_{pp}}\eta, \tag{7}$$

which is constant for the same geometry and fluid and independent of H.

When $H \to 0$, then $a_h \to \infty$ and this simple rheological shift factor diverges. An alternate definition for shift factor that incorporates the characteristic roughness of the fixtures is

$$a_h = \frac{R}{H + \epsilon}, \tag{8}$$

where ϵ is the r.m.s roughness of the plates under zero load conditions. We show below that this simple definition of the shift factor correctly captures the measured variations in the tribo-rheometry data throughout the hydrodynamic lubrication region. We recognize that in the mixed lubrication regime a more realistic elastohydrodynamic lubrication (EHL) model would incorporate variations in ϵ with the normal stress and the Young's modulus of the fixture material (see for example [14, 15]). However, we do not seek to shift or superpose our results in this regime.

To carry out the superposition, the experimental data for $H = 300\mu$m is used as the reference curve. The average roughness of plates is less than 1μm and the shift factor for this case is calculated to be $a_h = 0.01/301 \times 10^{-6} = 33.22$. All of the other results for different gaps and normal forces are then superimposed onto this shifted reference data. Despite knowing the nominal gap size for each set of rheology data, we choose not to use the gap size to calculate the shift factor. The shift factors are determined from the measured data by finding the required multiplier to superimpose the measured torque values with the reference data through an iterative method. The shifted results are shown in figure 2(b). On the ordinate axis of this figure we show the net torque divided by the radius which has units of μN and is analogous to the lateral force that would be measured in a pin-on-disk tester.

As mentioned in the introduction, alternate ways of presenting such data have been suggested by Luengo et al. [10] in order to create generalized 'friction maps'. In figure 2(c), the horizontal axis represents the shear rate in the fluid, $\dot{\gamma}_R = \Omega a_h$. On the ordinate axis we

show the effective viscosity, η_{eff} which is defined as:

$$\eta_{eff} = \frac{1}{\Omega a_h}\tau_R. \tag{9}$$

For the larger gap sizes, the effective viscosity is constant as expected for a Newtonian fluid and it is equal to the bulk viscosity as shown in figure 2(c). Under fixed load conditions, the data at high rotation rates can also be shifted onto this curve. However at the lower shear rates and high normal forces, the tribology results show that the effective viscosity is not constant but has a power-law function of $\eta_{eff} \sim \dot{\gamma}_R^{-n}$ where $n \approx 1.0$. This is within the range of values reported by Luengo and coworkers [10] and in agreement with the 'universal' value of $n = 0.9 \pm 0.1$ recently computed by Yamada [16].

From the definition in equation (8), the calculated values of the inverse of the shift factor should vary linearly with the gap according to

$$\frac{1}{a_h} = \frac{1}{R}H + \frac{\epsilon}{R}. \tag{10}$$

Linear regression of the data for five largest gap settings to this function gives the best fit $1/a_h = 9.3 \times 10^{-5}H + 4.5 \times 10^{-4}$ with ${\mathrm{R_{corr}}}^2 = 0.967$. These values are close to the expected theoretical values of $1/R = 1.0 \times 10^{-4}$ and $\epsilon/R = 10^{-4}$. In figure 2(d) the inverse of the shift factor is plotted as a function of $H + \epsilon$ (in micrometers) on a double-logarithmic scale in order to better show the range of data. The first two data points (filled symbols) were not used in the regression above and represent the shift factors obtained from the tribological results at nominally 'zero gap'. The calculated values of the shift factor can only be placed on this linear curve through selection of an appropriate value for the 'effective gap'. The corresponding gap sizes from the linear regression above are 2μm and 5μm for normal forces

of 20N and 5N which is very reasonable.

3.2 Capabilities of The Tribo-rheometer

Having demonstrated the ability of the tribo-rheometry fixture to measure both conventional rheological properties in addition to frictional properties, we now briefly demonstrate the robustness of this approach. These results are presented uniformly in the form of Stribeck diagrams which can be obtained using the procedure defined in section 2. The results can also be reported in the form of generalized 'friction maps' if desired using the data analysis protocols above.

3.2.1 Effect of surface roughness

To explore the effect of surface roughness, we use fixtures made from three different materials. A roughened copper disk ($\epsilon = 678.7$nm), a smooth copper disk ($\epsilon = 93.1$nm), and a glass annulus machined from a $\lambda/20$ optical flat ($\epsilon = 0.7$nm). The r.m.s surface roughness of these surfaces are measured using a contacting surface profiler (P10 Tencor Inc.). The copper disks have the same radii and stress factor as reported in Section 3.1. The glass annulus has radii $R_1 = 2.25$cm, $R_2 = 2.54$cm and the stress factor of this system is calculated to be $SF_{ann} = 2\bar{R}/\pi(R_2^4 - R_1^4) = 0.10\text{cm}^{-3}$. The test fluid is Pennzoil 80W-90 with a measured zero shear viscosity of $\eta_0 = 0.70 \pm 0.08$ Pa s and we have used a 3cm diameter stainless steel top plate with the annulus fixture and 1 cm diameter stainless steel plate for disk fixture. The applied normal force is set at $F_N = 10.0 \pm 1.0$N and the experimental results

are shown in figure 3. At very low rotation rates, in the boundary lubrication region, the coefficient of friction is approximately constant in each experiment, with $\mu_{glass} < \mu_{copper}$. The differing roughness values of the two copper fixtures is irrelevant in this regime since the upper and lower surfaces are in intimate contact in each case. At very high rotation rates, all three curves fall on a single line with slope of 1.0 characteristic of hydrodynamic lubrication. However, in the mixed lubrication regime, the coefficient of friction is a strong function of the surface roughness, and the maximum decrease in μ arises for the roughest surface. The crossover from mixed lubrication to hydrodynamic lubrication also occurs at increasingly high Gumbel numner (or shear rate) as the r.m.s roughness decreases.

3.2.2 Effect of the lubricant fluid

Three different commercial lubricant are used to demonstrate the effect of fluid composition on the tribology of a system. We choose Pennzoil 80W-90 (□), Mobil1 75W-90 synthetic oil (○), and Castrol 80W-90 (●) as working fluids. The zero-shear rate viscosities of these fluids are measured to be 0.70 ± 0.08, 0.42 ± 0.14, and 0.81 ± 0.18 Pa s, respectively. These fluids are selected for triborheological comparison due to their similar viscosities and common industrial application (gear lubricant). The lower fixture is a roughened copper disk ($R =$ 1cm, $SF_{pp} = 0.64\text{cm}^{-3}$). The normal force is set to be 10N, corresponding to a normal stress of $\sigma = 3.2 \times 10^4 \text{N/m}^2$. As shown in figure 4, the triborheological properties of these fluids are quite distinct. The coefficient of friction of the Castrol oil is consistently higher ($\mu = 0.14 \pm 0.03$) than the values of the Mobil1 and Pennzoil fluids ($\mu = 0.11 \pm 0.04$). The transition to the mixed lubrication regime also starts at noticeably higher Gu for the Mobil1

synthetic oil compared to the other fluids. Finally, in the hydrodynamic part of the Stribeck diagram the curves are almost the same, with small variations consistent with the differing shear viscosities.

3.2.3 Effect of the normal force

Finally, the effect of variations in the applied load or normal force is shown in figure 5. The frictional properties of the Pennzoil 80W-90 fluid are tested using a rough copper fixture ($\epsilon = 678.7$nm, $SF_{pp} = 0.64\text{cm}^{-3}$) with two different preset normal force of 10N ($\square$) and 20N ($\circ$). The resulting Stribeck curves have the same qualitative features but do not completely superpose. In the boundary lubrication regime, the measured coefficients of friction for each imposed load vary by less than 10 percent; however, in the mixed and hydrodynamic regimes, doubling the normal force shifts the data towards the left of the diagram by a factor of two. This is in fact consistent with the earlier results shown in Figures 2(b) and 2(c). At larger applied loads the effective mean gap between the plates is smaller, or equivalently the gap- and load-dependent shift factor a_h that is required to shift the tribology data onto a rheological master curve of the effective viscosity η_{eff} is larger.

4 Future directions

In this letter, we have introduced a new triborheometry fixture that can be utilized with a torsional rheometer to measure the frictional properties of a fluid-solid pair as the sample

gap and applied load is varied. The instrument enables a wide range of rotation rates to be imposed, and by varying the contact area of the lower fixture, a wide range of normal stresses can also be attained. The results can be represented in the form of a conventional Stribeck curve, or in terms of a more general 'friction map' of the gap- and load- dependent effective viscosity of the fluid.

There are a number of possible applications for this system in both industrial and academic research environments. The device uses very small volumes of test fluid, and the construction material of the lower annulus or disk can be readily interchanged. It is thus possible to investigate the effects of surface patterning (lithographic or machined), the frictional properties of multilayer coatings and even the use of substrates comprised of living cells or tissue scaffolds grown on perfusion membranes.

As an example, we consider here the triborheological properties of two bio-lubricants commonly utilized in hip and knee joint arthroplasty. These preliminary tests with the triborheometer are performed using a 2 cm diameter stainless steel plate and a copper disk ($\epsilon = 678.7$nm, $SF_{pp} = 64\text{cm}^{-3}$) as a lower fixture to represent a typical metal-on-metal assembly [17]. further experiments are presently being performed using machined polyethylene annuli as the lower fixture surface. The test fluids considered are bovine serum and a solution of hyaluronic acid (HA) which is a major constituent of synovial fluid [18, 19]. Bovine serum ($\eta_0 = 0.02$ Pa s) is commonly used as a lubricant in laboratory pin-on-disk wear testing. The synthetic HA ($\eta_0 = 2.0$ Pa s) used in this experiment is of high molecular weight (2.2 MDa) and more highly concentrated (10 mg/ml) than typical in vivo joint fluid. Stribeck curves from these tests are presented in figure 6. The normal force for the HA test is 15N

(corresponding to a normal stress of $\sigma = 4.8 \times 10^4 N/m^2$), and for the bovine serum test is 5N ($\sigma = 1.6 \times 10^4 N/m^2$). The hydrodynamic, mixed, and boundary lubrication regions are all captured in these tests. The large lateral shift to higher Gu for the HA solution arises because of the larger zero-shear-rate viscosity of the solution; the actual angular velocities of the two tests span similar ranges. At a linear velocity of $(\Omega R)_{min} = 3.6 \times 10^{-3}$ m/s, the HA solution reaches a minimum friction coefficient of $\mu_{min} \approx 0.1$ which is a factor of two lower than the minimum friction observed in the bovine serum lubricant.

The food and consumer product industries also offer numerous future opportunities for triborheometry in quantifying concepts such as lubricity and astringency. High shear rates and narrow gaps are characteristic of many end-use applications including chewing of food stuffs [9] and application of skin creams or topical ointments [8]. By utilizing the Peltier plate located below the lower plate of the device, we can perform tests at controlled temperatures from $0°C \leq \theta \leq 95°C$. An external solvent trap can also be utilized if solvent evaporation or environmental humidity is of potential concern. To explore these additional capabilities, triborheometrical studies of model chocolate systems at a standardized test temperature of 40°C are presently underway.

This research was supported by PPG Industries. We would like to thank Prof. Howard Stone for numerous helpful discussions.

References

[1] E. Meyer, R.M. Overney, K. Dransfeld, and T. Gyalog. *Nanoscience: Friction and Rheology on the Nanometer Scale*, volume 1. World Scientific, Singapore, 1998.

[2] B Bhushan. *Fundamentals of Tribology and Bridging the Gap Between the Macro and Micro/Nanoscales*, volume 10 of *NATO/ASI Science Series: Mathematics, Physics and Chemistry*. Kluwer, Boston, 2000.

[3] M. Scherge and S.S. Gorb. *Biological Micro- and Nano-Tribology*. Springer-Verlag, Berlin, 2001.

[4] B. Bhushan, J.N. Israelachvili, and U. Landman. Nanotribology: friction, wear and lubrication at the atomic scale. *Nature*, 374:607–616, 1995.

[5] J. Klein, Y. Kamiyama, H. Yoshizawa, J.N. Israelachvili, G.H. Fredrickson, P. Pincus, and L.J. Fetters. Lubrication forces between surfaces bearing polymer brushes. *Macromolecules*, 26:5552–5560, 1993.

[6] H. Czichos. Tribology and its many facets: from macroscopic to microscopic and nanoscale phenomena. *Meccanica*, 36:605–615, 2001.

[7] T.E. Karis and M.S. Jhon. The relationship between PFPE molecular rheology and tribology. *Trib. Lett.*, 5:283–286, 1998.

[8] R. Brummer and S. Godersky. Rheological studies to objectify sensations occurring when cosmetic emulsions are applied to the skin. *Coll. Surf. A.*, 152:89–94, 1999.

[9] S. Lee, P. Heuberger, M.and Rousset, and N.D. Spencer. Chocolate at a sliding interface. *J. Food Science*, 67(7):2712–2717, 2002.

[10] G. Luengo, J.N. Israelachvili, and S. Granick. Generalized effects in confined fluids: new friction map for boundary lubrication. *Wear*, 200:328–335, 1996.

[11] Y.Z. Hu and S. Granick. Microscopic study of thin film lubrication and its contributions to macroscopic tribology. *Trib. Lett.*, 5(1):81–88, 1998.

[12] A. Mukhopadhyay and S. Granick. Micro- and Nano-rheology. *Curr. Opin. Colloid Interface Sci.*, 6:423–429, 2001.

[13] R.B. Bird, R.C. Armstrong, and O. Hassager. *Dynamics of polymeric liquids*. John Wiley & Sons, Inc., New York, USA, 1987.

[14] E.R.M. Gelnick and D.J. Schipper. Calculation of Stribeck curves for line contact. *Trib. Int.*, 33:175–181, 2000.

[15] E. Brodsky and H. Kanamori. Elastohydrodynamic lubrication of faults. *J. Geophys. Res.*, 106:16357–16374, 2001.

[16] S. Yamada. General shear-thinning dynamics of confined fluids. *Trib. Lett.*, 13(3):167–171, 2002.

[17] S.L. Smith, D. Dowson, and A.A.J. Goldsmith. The lubrication of metal-on-metal total hip joints: a slide down the Stribeck curve. *Proc. Instn. Mech. Eng.*, 216:483–493, 2001.

[18] Y. Zhu and S. Granick. Biolubrication: Hyaluronic acid and the influence on its interfacial viscosity of an antiinflamatory drug. *Macromolecules*, 36:937–976, 2003.

[19] D. Mazzuco. *Variation in joint fluid composition and its effect on the tribology of replacement joint articulation.* PhD thesis, Massachusetts Institute of Technology, Cambridge, Massachusetts, USA, 2003.

Figures captions:

Figure 1: The schematic of the tribo-rheometer and its fixtures.

Figure 2: Gap effect on the measurements. (a) The measured torques for radial velocity sweep for different gap sizes of 300 μm, ($\triangle$); 200 μm, ($\blacktriangle$); 100 μm, ($\square$); 80 μm,($\blacksquare$); 50 μm, ($\bigcirc$); and 20 μm, ($\bullet$); and normal forces of 5 N, (+), and 20 N, ($\times$). (b) Same results which hydrodynamic parts are superimposed using a shift factor, a_h. The abscissa is torque divided by the radius of the fixture. (c) Same data presented as 'friction map'. The effective viscosity, η_{eff} , is plotted as a function of the shear rate. (d) The inverted of the calculated shift factor, $1/a_h$, is plotted as a function of the gap size, H. The solid line is the linear fit to the data. The solid points are from the tribology tests and only shown for comparison.

Figure 3: The effect of surface roughness on tribology is shown on a Stribeck diagram. Rough copper ($\bullet$), smooth copper ($\square$), and glass ($\circ$) are tested with Pennzoil 80W-90 lubricant and normal force of 10N.

Figure 4: The effect of lubricant fluid on tribology is shown on a Stribeck diagram. Castrol 80W-90 ($\bullet$),Mobil1 75W-90 synthetic oil ($\circ$), and Pennzoil 80W-90 ($\square$) are tested on a copper fixture with normal force of 10N.

Figure 5: The effect of normal force on tribology is shown on a Stribeck diagram. Pennzoil 80W-90 lubrication oil are used on copper fixture with normal force of 10N ($\circ$), and 20N ($\square$).

Figure 6: Stribeck diagram for Bovine serum ($\bullet$) and hyaluronic acid ($\circ$) on a copper fixture.

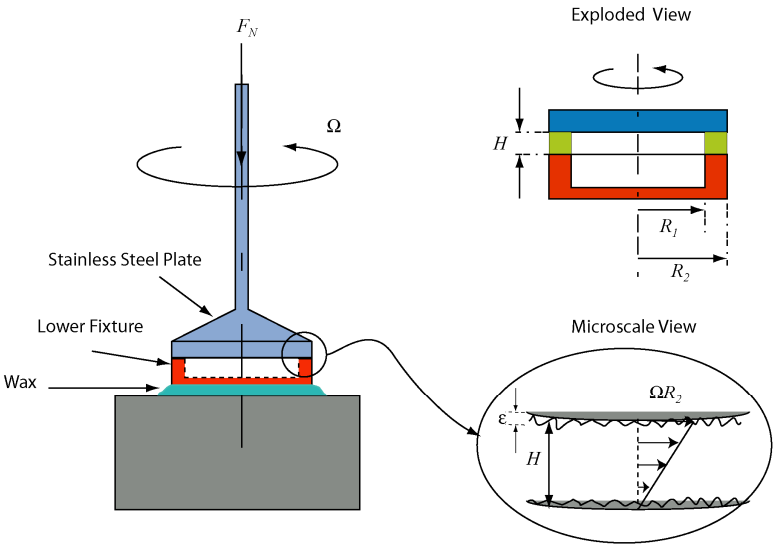
F_N
Ω
Stainless Steel Plate
Lower Fixture
Wax
Exploded View
H
R_1
R_2
Microscale View
ΩR_2
ε
H

Figure 1:

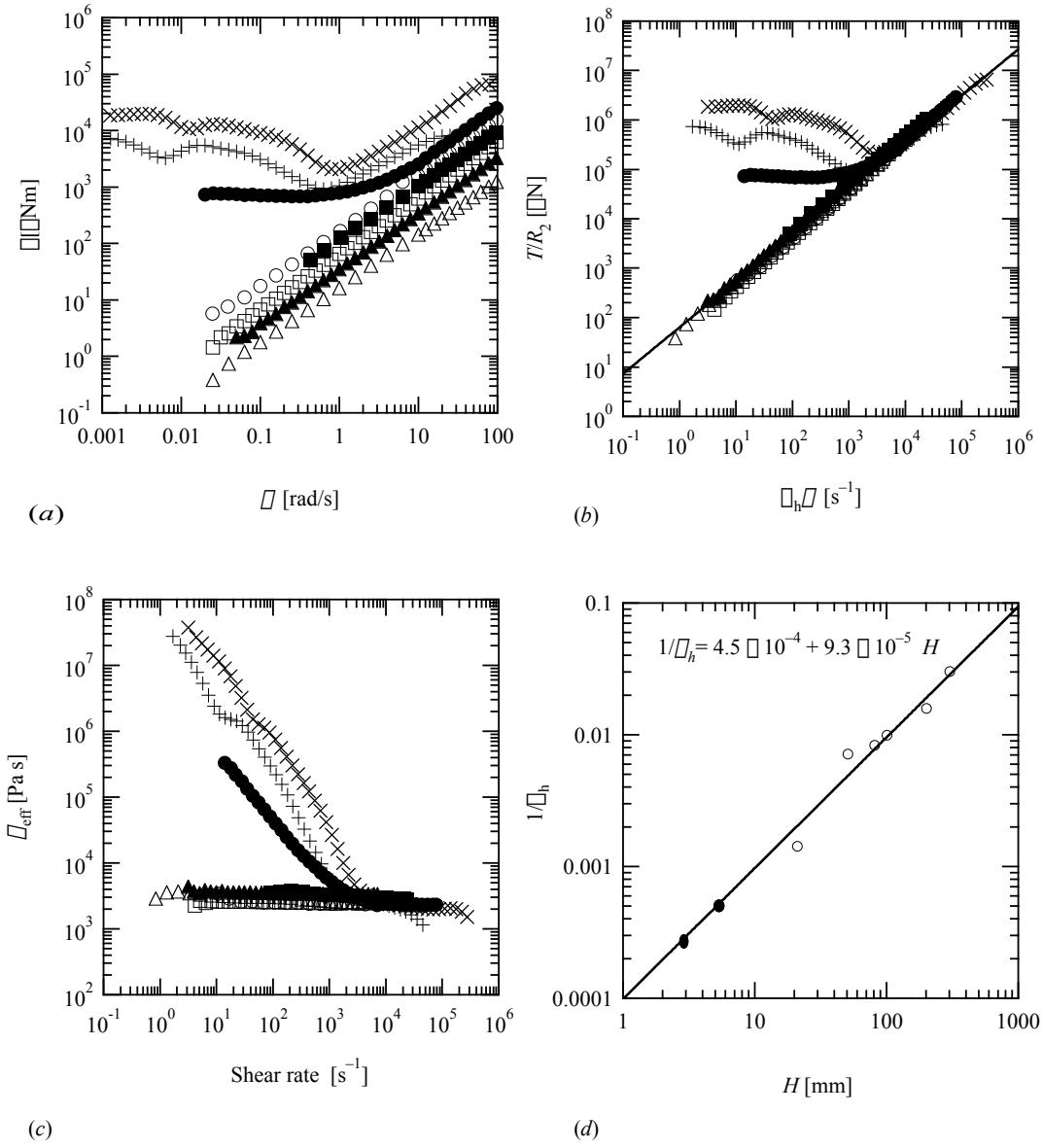
(a)
(b)
(c)
(d)
[rad/s]
T/R_2 [N]
$\dot{\gamma}_h$ [s^{-1}]
η_{eff} [Pa s]
Shear rate [s^{-1}]
$1/\eta_h = 4.5 \times 10^{-4} + 9.3 \times 10^{-5}$ H
$1/\eta_h$
H [mm]

Figure 2:

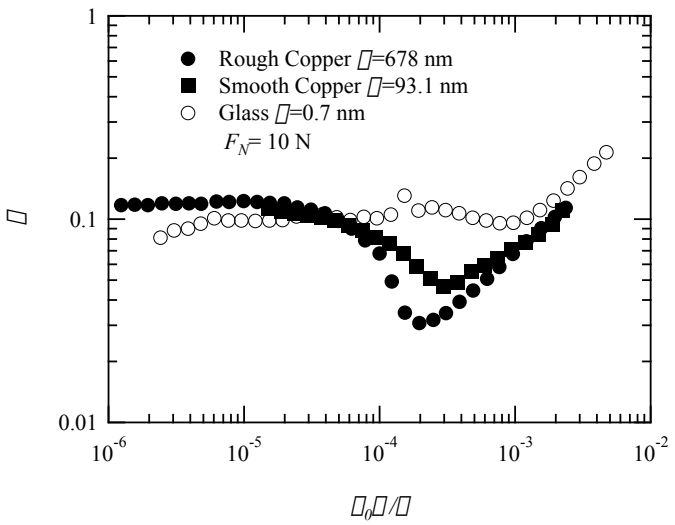
1
0.1
0.01
Rough Copper σ=678 nm
Smooth Copper σ=93.1 nm
Glass σ=0.7 nm
F_N= 10 N
μ
10^{-6}
10^{-5}
10^{-4}
10^{-3}
10^{-2}
$v_0\tau/\sigma$

Figure 3:

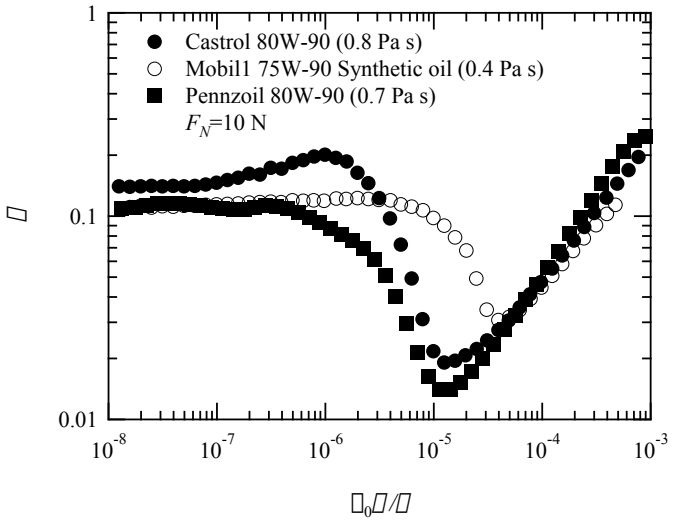
Castrol 80W-90 (0.8 Pa s)
Mobil1 75W-90 Synthetic oil (0.4 Pa s)
Pennzoil 80W-90 (0.7 Pa s)
F_N=10 N
1
0.1
0.01
10^{-8}
10^{-7}
10^{-6}
10^{-5}
10^{-4}
10^{-3}

Figure 4:

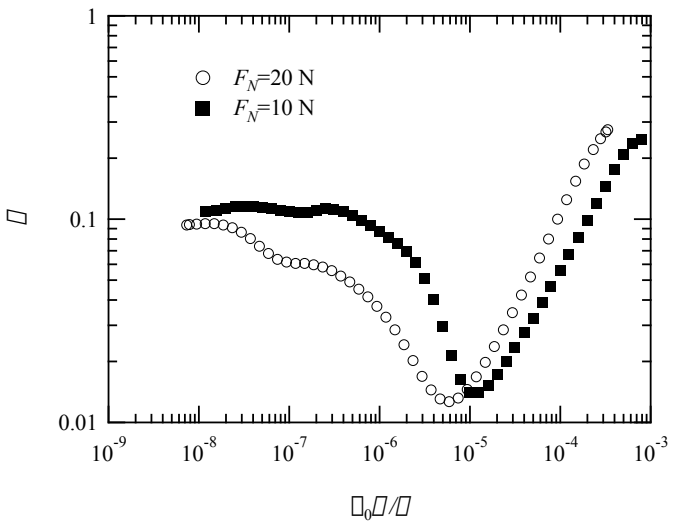

Figure 5:

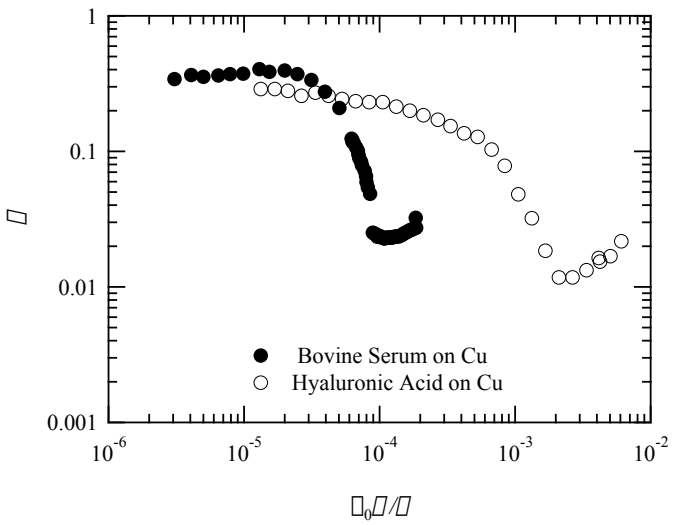
1
0.1
0.01
0.001
10^{-6}
10^{-5}
10^{-4}
10^{-3}
10^{-2}
Bovine Serum on Cu
Hyaluronic Acid on Cu

Figure 6: